Journal of ELECTRONIC MATERIALS, Vol. 49, No. 9, 2020
https://doi.org/10.1007/s11664-020-08081-2
© 2020 The Minerals, Metals & Materials Society

TOPICAL COLLECTION: 18TH CONFERENCE ON DEFECTS (DRIP XVIII)

Electron-Beam-Induced Current Study of Dislocations and Leakage Sites in GaN Schottky Barrier Diodes

JUN CHEN,[1,4,7] WEI YI,[1,4] ASHUTOSH KUMAR,[1,5] AKIO IWANADE,[1] RYO TANAKA,[2] SHINYA TAKASHIMA,[2] MASAHARU EDO,[2] SHUN ITO,[3] TAKASHI KIMURA,[1,4] TADAKATSU OHKUBO,[1,5] and TAKASHI SEKIGUCHI[1,6]

1.—Research Network and Facility Services Division, Center for GaN Characterization and Analysis, National Institute for Materials Science, Tsukuba 305-0047, Japan. 2.—Advanced Technology Laboratory, Fuji Electric Co. Ltd., Hino, Tokyo 191-8502, Japan. 3.—Institute for Materials Research, Tohoku University, Sendai 980-8577, Japan. 4.—International Center for Materials Nanoarchitectonics, National Institute for Materials Science, Tsukuba 305-0044, Japan. 5.—Research Center for Magnetic and Spintronic Materials, National Institute for Materials Science, Tsukuba 305-0047, Japan. 6.—University of Tsukuba, Tsukuba 305-8577, Japan. 7.—e-mail: CHEN.Jun@nims.go.jp

This work aims to clarify the electrical activities of threading dislocations and their relation with leakage sites in homoepitaxial GaN Schottky barrier diodes based on the electron-beam-induced current (EBIC) technique and transmission electron microscopy (TEM). First, the recombination activities of threading dislocations in epilayers grown on different substrates are compared by EBIC. The dislocation type is characterized based on etch pit measurements and TEM. The dislocation density and character are strongly affected by defects in the substrate. The recombination strength of dislocations is revealed to be correlated with their type. It is found that single dislocations including both edge and mixed type exhibit weak ($< 5\%$) EBIC contrast, while dislocation clusters show strong contrast (up to 30%). Second, leakage sites in Schottky diodes are visualized by EBIC under reverse bias. There is no direct correlation between the initial leakage sites and threading dislocations; whereas, instead of dislocations, a variety of initial leakage/breakdown sites are found, including grown-in pit defects as initial breakdown sites and hillocks at the Schottky interface acting as strong leakage sites.

Key words: EBIC, TEM, GaN, dislocations, leakage sites

INTRODUCTION

Wide-bandgap materials are now attracting great research interest for use in future power electronics.[1] In particular, GaN-based power devices are promising candidates that benefit from the figure of merit of this material. GaN-on-GaN vertical structures have been proposed due to their advantages in terms of large current flow and high breakdown voltage.[2] Vertical GaN *p*–*n* junction diodes with high breakdown voltages above 4 kV have also been reported.[3,4] With the progress in GaN growth techniques, large-size GaN substrates with low dislocation density have become possible. The dislocation density has been reduced from previous values of 10^8 cm^{-2} to 10^9 cm^{-2} to the present range of 10^4 cm^{-2} to 10^6 cm^{-2}. Hydride vapor-phase epitaxy (HVPE) is used commercially to grow large-size GaN substrates because of its high growth rate and high purity. Many efforts have been made to suppress the dislocation density, including special technologies such as epitaxial lateral overgrowth

(Received November 29, 2019; accepted March 13, 2020; published online March 26, 2020)

(ELOG)[5] and dislocation elimination by epitaxial growth with inverse-pyramidal pits (DEEP).[6] These methods can help to eliminate dislocations within a large area, but leave the issue of a nonuniform distribution of dislocations. To achieve a low density and uniform distribution, new methods such as HVPE based on nanovoid-assisted separation[7] and dislocation- and strain-free growth on unique GaN nanowire templates[8,9] have been developed.

However, at present, HVPE GaN substrates still contain a relatively high density of dislocations, which would propagate into the epilayer during epitaxial growth using the metalorganic vapor phase epitaxy (MOVPE) technique. The presence of threading dislocations could result in charge traps or leakage sites, resulting in device degradation and failure. Several works based on a variety of characterization methods have been reported. It has been found using ballistic electron emission microscopy that threading dislocations with a screw component are accompanied by high current densities and low effective Schottky barrier heights.[10] Conductive atomic force microscopy (C-AFM) study has suggested that there are two kinds of leakage current paths, viz. open-core screw and pure screw dislocations,[11] and a model of oxygen-related defect centers in the bandgap has been proposed as the origin of the leakage current. More recently, it was reported based on emission microscopy and etch pit studies that pure screw dislocations are related to the reverse leakage in vertical GaN *p*–*n* diodes.[12]

Threading dislocations in GaN epilayers can be structurally clarified into three categories: edge type with Burgers vector b of 1/3 <11-20>, screw type with b of <0001>, and mixed type with b of 1/3 <11-23>.[13] The dislocation type can be determined by wet chemical etching, since the shape and size of the etch pit varies with the dislocation type.[14–16] Among various etching methods, molten KOH etching is well developed for delineating dislocations in GaN. Generally, the size of etch pit is in the sequence of screw > mixed > edge.[17] A more precisely way is to image dislocation with different diffraction vectors in transmission electron microscopy (TEM) and do $\boldsymbol{g}{\cdot}\boldsymbol{b}$ analysis to determine Burgers vector.[18]

On the other hand, to investigate the electrical properties of dislocations, most studies are limited to optical characterizations of dislocations in GaN substrates based on cathodoluminescence (CL) and photoluminescence (PL).[19–21] Dislocations are usually regarded as nonradiative centers and show dark contrast in CL images. However, there is controversy regarding the CL contrast of dislocations. It has been reported that screw-type dislocations showed no dark contrast in CL images, indicating recombination inactivity, while edge- and mixed-type dislocations are dark due to impurity getterers such as oxygen.[22] However, others have found that the CL contrast of screw-type dislocation tends to be darker than that of the edge or mixed type.[17] Dislocations may even be luminescent when accompanied by radiative centers related to point defects and/or dopant impurities.[23,24]

Optical characterization methods offer the advantages of contactless nature, fast testing, and the capability to distinguish radiative from nonradiative recombination centers. However, they can only indirectly describe the electrical activity of dislocations based on the CL contrast. From this viewpoint, electrical characterization based on the electron-beam-induced current (EBIC) technique is straightforward, since it monitors the current signal and the recombination contrast is obtained including both radiative and nonradiative recombination processes.[25,26] In the past, EBIC has been applied to extended defects such as grain boundaries and dislocations in silicon and oxide semiconductors.[27,28] Moreover, it could be directly applied to actual device structures and identify weak points related to device leakage and breakdown.[29,30] Early EBIC study on dislocations in GaN has also been reported in literature.[31] However, at that time, the density of dislocations in GaN grown on a foreign substrate was too high (over 10^8 cm^{-2}), making it impossible to image single dislocations due to the limited spatial resolution. Nowadays, with the rapid progress in GaN growth, dislocations have been greatly suppressed and EBIC images of single dislocations have become possible. The recombination activity of dislocations in GaN grown by different methods has been compared, leading to the conclusion that the recombination strength of dislocations is strongly dependent on the dopant concentration, while there is no obvious correlation between the dislocation activity and the growth method.[32]

Recently, we attempted to investigate the dislocations in homoepitaxial MOVPE GaN epilayers grown on different HVPE GaN substrates. It was noted that there exists a significant difference in the electrical activity of dislocations for the different substrates and also epilayers. However, the electrical properties of dislocations in the homoepitaxial GaN layer are not well understood, and the role of dislocations in current leakage/breakdown remains unclear. We report herein an EBIC investigation of the recombination activities of dislocations in homoepitaxial GaN epilayers grown on different HVPE substrates, and try to correlate the electrical properties with the dislocation type. The initial leakage sites in a GaN Schottky barrier diode (SBD) could be monitored by bias-dependent EBIC imaging, and the relationship between the dislocations and initial leakage sites clarified.

EXPERIMENTAL PROCEDURES

Two groups of GaN Schottky diodes (SBD-I and SBD-II) fabricated on epilayers grown on two different HVPE substrates (substrate I & substrate II) were comparatively investigated. Both substrates were *n*-type Si-doped with carrier

concentration of 1.75×10^{18} cm^{-3}. The difference is the distribution and density of dislocations. Substrate I was grown from a patterned template, involving facet growth. The dislocations were convergent to the core of the facet growth and thus exhibited a nonuniform distribution. The dislocation density varied from 10^8 cm^{-2} to 10^5 cm^{-2}. Substrate II had homogeneously distributed dislocations with density of 10^6 cm^{-2}. A GaN epilayer with thickness of 4 μm was grown epitaxially on each kind of substrate by MOVPE. The epilayers were also n-type Si-doped with carrier concentration of 1.5×10^{16} cm^{-3}. Schottky contacts were prepared on the epilayers by deposition of Ni to thickness of 150 nm and covered by a Au layer with thickness of 50 nm by a lift-off process. Backside Ohmic contacts were prepared by deposition of Ti/Al onto the substrates.

EBIC measurements were carried out using a JEOL JSM-7600F field-emission scanning electron microscope (FE-SEM) at room temperature. Kleindiek micromanipulators installed inside the SEM chamber were used to form electrical connections for I–V and EBIC measurements. I–V testing was performed using a Keithley S4200 semiconductor characterization system. EBIC images were recorded at accelerating voltage of 5 kV to 20 kV. The dependence on the accelerating voltage can provide depth information from the Schottky interface to the bulk region. Defects at the Ni/GaN Schottky interface could be visualized at lower accelerating voltage, while dislocations start to be visible in EBIC with dark recombination contrast when the accelerating voltage is larger than 15 kV. The EBIC contrast is defined as

$$C = (I_\mathrm{b} - I_\mathrm{d})/I_\mathrm{b}, \tag{1}$$

where I_b and I_d are the EBIC current at the background and dislocation, respectively. Monitoring of initial leakage sites is possible by EBIC imaging under reverse bias.

After EBIC, the dislocation type was analyzed based on etch pits and $\boldsymbol{g}{\cdot}\boldsymbol{b}$ analysis in TEM. For wet chemical etching, the electrode layers were removed by rinsing in aqua regia, and threading dislocations in the epilayer were etched by molten KOH with 1 wt.% Na_2O_2 at 510°C in a carbon crucible. The dislocation below an etch pit was picked up by focused ion beam (FIB) and observed in TEM. The Burgers vector $\boldsymbol{b}$ of a threading dislocation can be found based on $\boldsymbol{g}{\cdot}\boldsymbol{b}$ analysis in two-beam conditions. TEM observation of dislocations was performed using a FEI Tecnai G^2 20 microscope with double-tilt holder at 200 kV. TEM observation of initial leakage sites was also performed. Different from dislocation analysis, a leakage site in a Schottky diode may be associated with interface defects, thus the specimen was fabricated by FIB with the electrode metal layers left. TEM observation of leakage sites was carried out using a high-resolution transmission electron microscope (TOPCON EM-002BF) with an energy-dispersive spectrum (EDS) detector at 200 kV.

RESULTS AND DISCUSSION

EBIC Study of Recombination Activity of Threading Dislocations

First, the electrical recombination activities of threading in epilayers grown on the different substrates were investigated. For this purpose, the accelerating voltage was set at 20 kV, which corresponds to an electron range of about 1 μm. The depletion region width was about 200 nm. Beneath the depletion region, dislocations act as active recombination centers of minority carriers and show dark EBIC contrast. Figure 1 shows typical EBIC images of threading dislocations in the two groups of SBD specimens. In SBD-I, individual dark spots and clusters related to single and bundled dislocations were observed, while in SBD-II, only individual dark spots were seen. The single dislocation shows an EBIC contrast of 5%, while the bundled one shows strong contrast of up to 30%. The different EBIC appearance of threading dislocations is affected by the defects in the substrates. As mentioned above, substrate I was grown from a patterned template, involving facet growth. This special growth technique is utilized to eliminate dislocations within a large area by dislocation convergence towards the center, so the distribution of dislocations is inhomogeneous. The cluster observed in the EBIC image correlates with the center point of the dislocation convergence. Threading dislocations in the epilayer grown on substrate I exhibited a similar inhomogeneous distribution due to the propagation of dislocations from the substrate. On the other hand, the grown-in dislocations in substrate II were uniformly distributed with low average density, which results in the homogeneous distribution of threading dislocations in the epilayer.

Figure 2 shows secondary-electron (SE) images of dislocation etch pits. In SBD-I, there are superlarge hexagonal pits (size over 10 μm). These superlarge pits correspond to the bundled dislocation clusters seen in Fig. 1a. At the dislocation clusters, overetching occurred and the substrate becomes visible. In addition to the superlarge pit, there are large, medium, and small etch pits with the shape of inverted hexagonal cones. These etch pits correspond to individual threading dislocations of screw, mixed, and edge type. In SBD-II, most of the etch pits were of small and medium size, corresponding to edge- and mixed-type dislocations. We extracted the dislocations below the small and medium etch pits by FIB and performed TEM observation at two diffraction conditions ($\boldsymbol{g}$ = 11–20 and $\boldsymbol{g}$ = 0002). The dislocation from the small-size etch pit was visible under 11–20 but became invisible under 0002 diffraction, while that from the medium-size etch

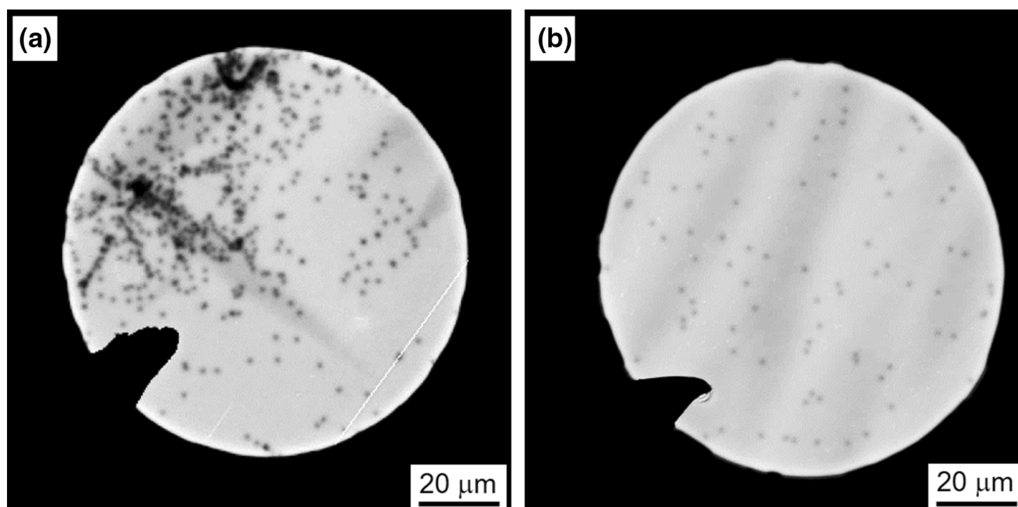

Fig. 1. EBIC images of dislocations in two groups of GaN SBD devices: (a) SBD-I with convergence of dislocations and (b) SBD-I with homogeneous distribution of dislocations.

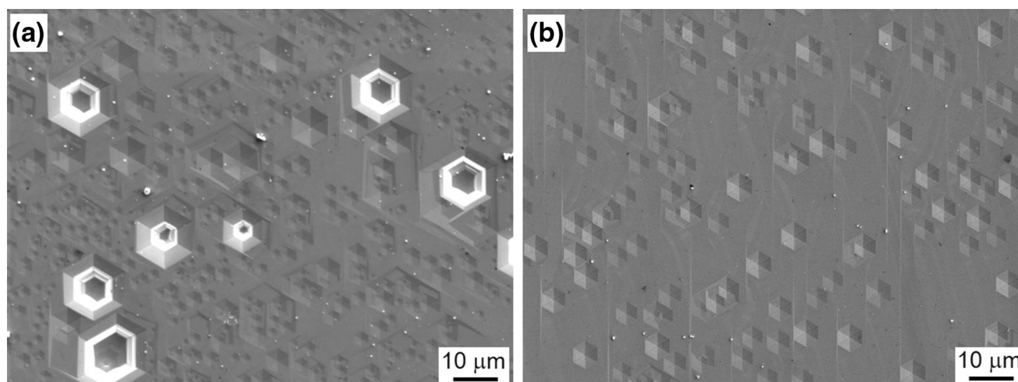

Fig. 2. SE images of dislocation etch pits in GaN epilayers grown on two different substrates: (a) substrate I and (b) substrate II.

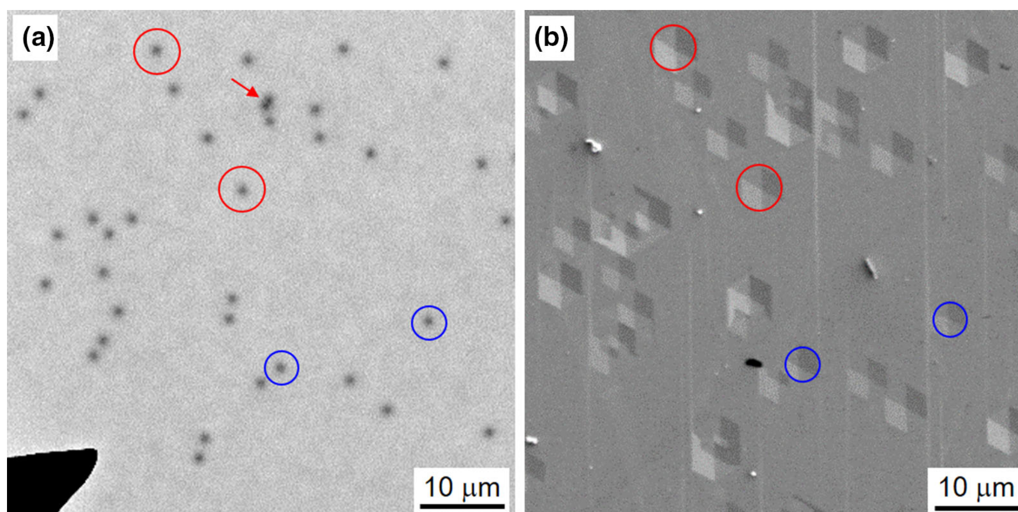

Fig. 3. Correspondence between EBIC image of dislocations (a) and SE image of etch pits (b) in epilayer on substrate II.

pit was visible under both diffraction conditions. This further confirms that the small etch pit was of edge type while the medium etch pit was of mixed type.

It is now possible to correlate the electrical activities of dislocations with their character. Figure 3 shows an EBIC image of dislocations in SBD-II and a corresponding SE image of etch pits at the same position. The dislocations marked by blue circles with small-size etch pits are of edge type, while those marked by red circles with medium-size etch pits are of mixed type. Note that the value of the EBIC contrast of all these dislocations is less than 5%. Considering the recombination activities, there is no significant difference between the edge- and mixed-type dislocations. Sometimes, we can also observe dislocations with slightly darker contrast of around 8–9%, as indicated by the arrow in Fig. 3a, which is probably due to double or multiple dislocations close to each other.

Leakage Sites Visualized under Biased EBIC

We attempted to correlate leakage sites with the dislocation density and distribution in the epilayers.

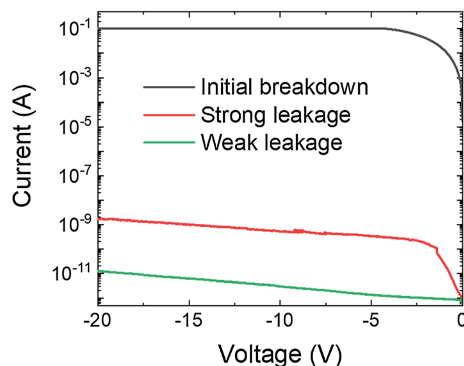

Fig. 4. *I–V* profiles of SBD-II showing different levels of current leakage, classified as initial breakdown, strong leakage, and weak leakage.

However, there was no direct correlation between the leakage sites and dislocations. Instead of dislocations, other factors affect the initial leakage current. In the following, the leakage sites in SBD-II are demonstrated based on *I–V* and bias-dependent EBIC observations. The *I–V* characteristics of SBDs with different leakage levels, termed initial breakdown, strong leakage, and weak leakage, are shown in Fig. 4. The initial breakdown diode shows Ohmic current–voltage characteristics; the strong leakage diode has a quick increase in the reverse current at the beginning of negative bias and exhibits a leakage current about two orders of magnitude higher than the weak leakage one.

Corresponding biased EBIC images of these diodes are shown in Fig. 5. The bias voltage is −0.1 V for the initial breakdown device and −5 V for the others. In the initial breakdown diode, a small bias such as −0.1 V can already result in an overload of the current signal in the EBIC current amplifier. The EBIC image shown in Fig. 5a suggests that a breakdown site occurs near the electrode edge. The appearance of a horizontal bright zone is always found when the e-beam scans over a strong leakage point. On the other hand, for the diodes before breakdown, leakage sites are found with bright EBIC contrast located either on the electrode periphery or within the inner region of the Schottky metal electrode. The lift-off process for metal electrode formation does not seem to be suitable for the EBIC evaluation of Schottky diodes in this study, since leakage occurs easily through weak points at the electrode edge.

Figure 6a–c shows SE and EBIC images of the initial breakdown diode. The EBIC image taken at 0 V does not show obvious leakage, but when applying a very small bias such as 0.01 V, leakage occurs and a bright zone is formed through the entire electrode, following the beam scanning direction. Figure 6d–f and d shows zoomed-in SE and EBIC images of the region marked in Fig. 6a. There are a few pit defects near the electrode edge. When

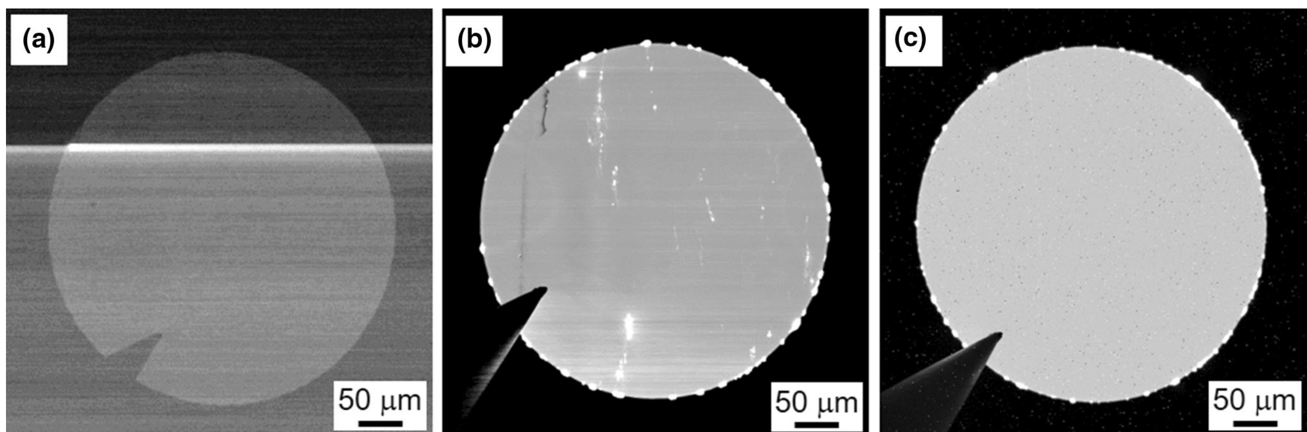

Fig. 5. EBIC images of SBD-II for different leakage levels: (a) initial breakdown, (b) strong leakage, and (c) weak leakage. The EBIC images are biased at −0.1 V for (a) and −5 V for (b) and (c).

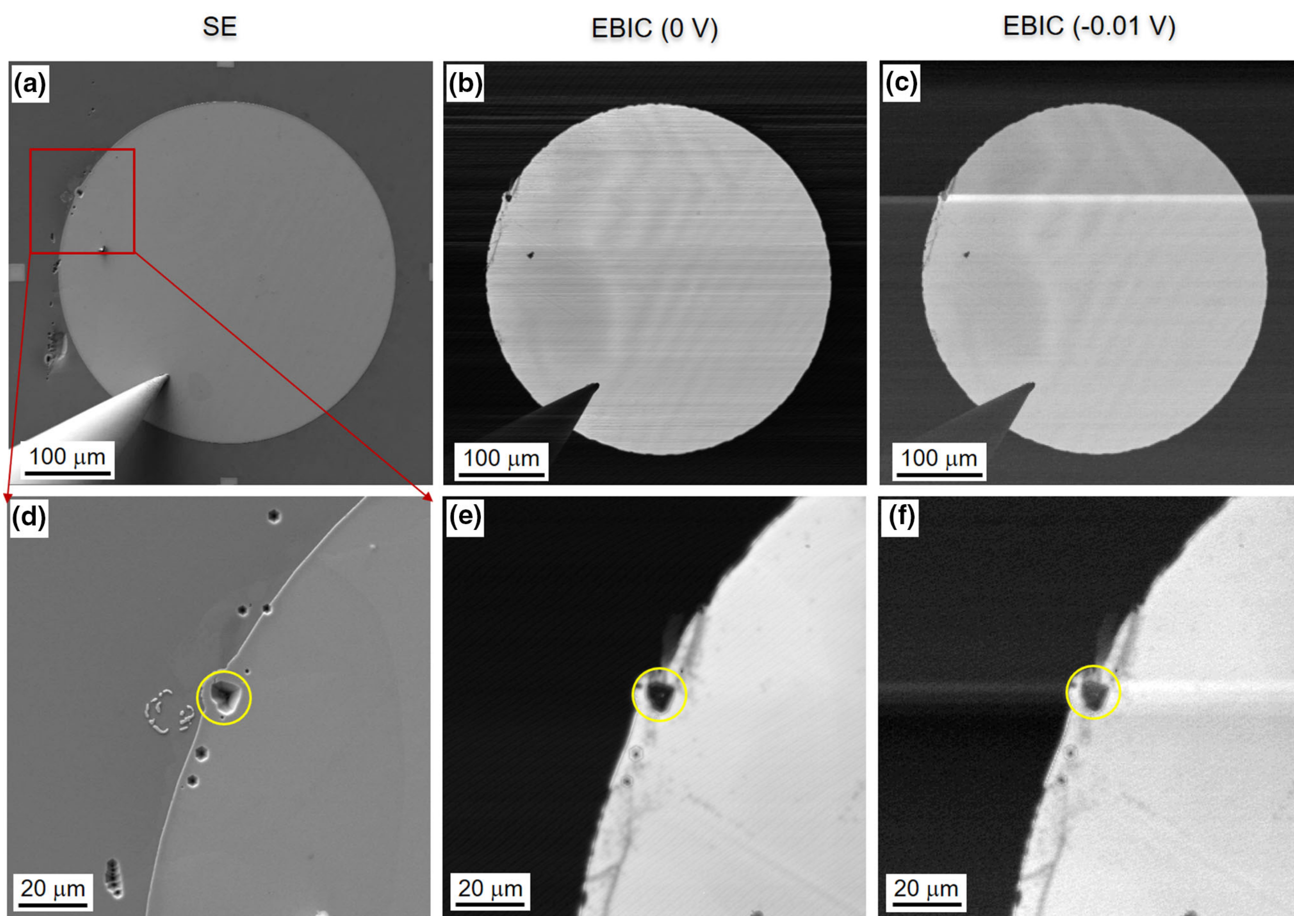

Fig. 6. (a) SE image, and EBIC images at (b) 0 V and (c) −0.1 V, of grown-in pit defects in the epilayer accounting for initial breakdown. Zoomed-in (d) SE image, and EBIC images at (e) 0 V and (f) −0.1 V, of the region marked in (a). (a) SE; (b) EBIC at 0V; (c) EBIC at -0.1 V; (d) SE; (e) EBIC at 0 V; (f) EBIC at -0.1 V.

biased at −0.01 V, an abrupt rise of the EBIC current started near the large-size pit defect, as shown in Fig. 6d. Note that the width of the bright zone is comparable to the size of the pit defect. The initial breakdown site is due to grown-in pit defects in the epilayer. In the growth of HVPE GaN films or substrates, pit defects are formed due to the difference in growth rate of different facets in case of the presence of dislocation clusters or impurity inclusions involved during growth.[33–35] Previous emission microscopy investigation of SBD devices has also found that pit defects in the epilayer would cause initial failure,[36] and the pit defects are associated with carbon impurities decorated at dislocations with a screw component. Although the density of pit defects in the epilayer is low, they are detrimental in power devices. In addition, a large-size pit defect tends to act as an initial breakdown site, while small-size pits do not. One consideration is that the bottom of a large pit has reached the highly doped substrate and formed a conductive path.

There is another kind of leakage site, which is more frequently found inside the Schottky region. At first, we thought that these leakage sites may correlate with threading dislocations. However, this assumption was overthrown by later EBIC and TEM studies. Figure 7 shows a Schottky region with both dislocations and leakage sites present. Dislocations appear as dark spots in the EBIC image at 0 V, but their contrast disappears when biased at −10 V. On the contrary, leakage sites (marked by dashed red circles) show weak bright EBIC contrast at 0 V but become brighter at −10 V. This suggests that the locations of these leakage sites are clearly different from the dislocations. The SE image in Fig. 7a shows that the locations with leakage sites appear slightly darker than the background region. A decrease in the yield of secondary electrons may take place due to the presence of a leakage path.

The origin of these leakage sites may be associated with defects close to the surface. To confirm this, EBIC observations were conducted at a low accelerating voltage of 10 kV, corresponding to an electron range of 200 nm, just at the interface of Ni and the GaN epilayer. Figure 8 compares the EBIC images taken at 20 kV and 10 kV, with either zero bias or negative bias of −3 V. It is found that dislocations are visible with dark contrast at 20 kV

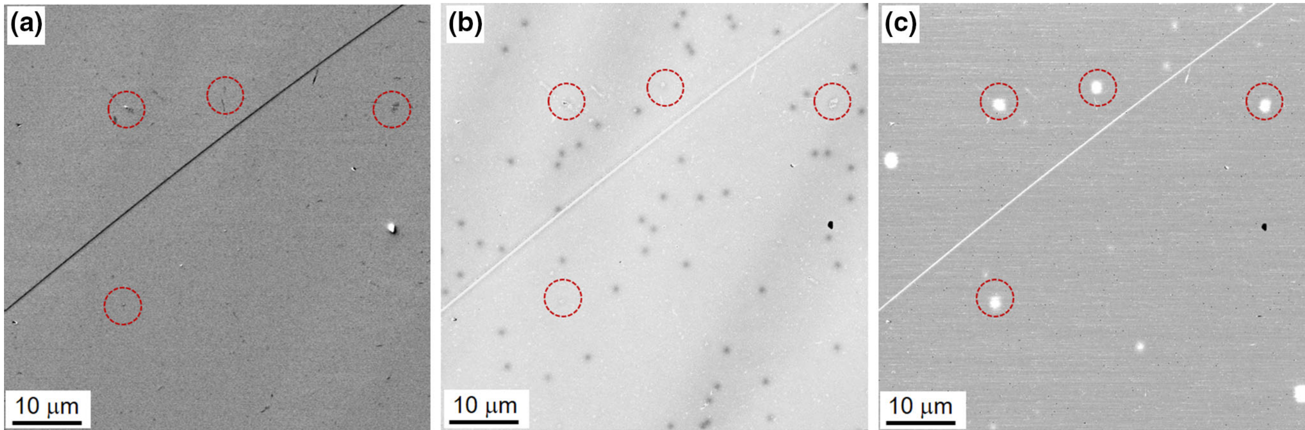

Fig. 7. SE and EBIC images of dislocations and leakage sites at the inner Schottky region: (a) SE, and EBIC at (b) 0 V with dislocations showing dark contrast and (c) −10 V with leakage sites showing bright contrast.

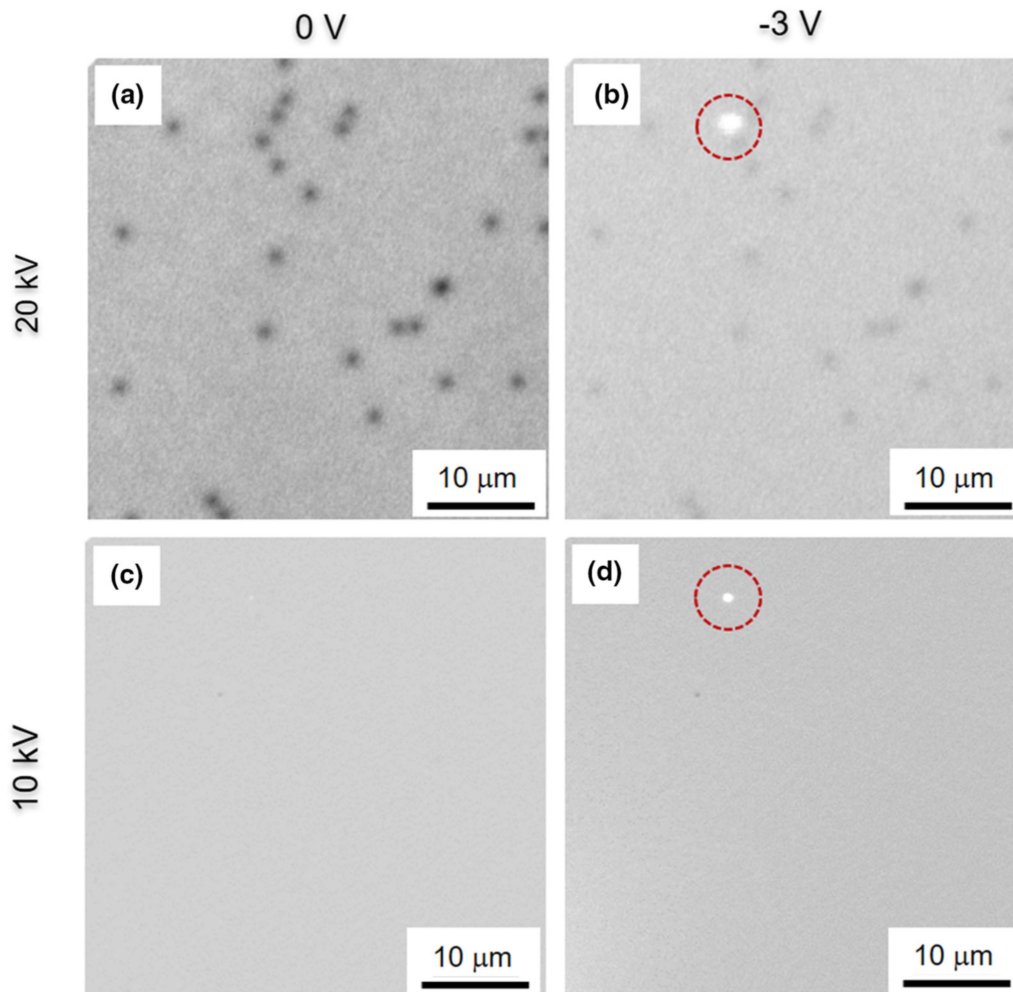

Fig. 8. Comparison of EBIC images taken at bias/accelerating voltages of (a) 0 V/20 kV, (b) −3 V/20 kV, (c) 0 V/10 kV, and (d) −3 V/10 kV.

but are not observed at 10 kV. On the other hand, the leakage site (marked by red circle in Fig. 8b and d) is visible with bright contrast at both 20 kV and 10 kV, indicating that it is near the surface.

After EBIC observation, the microstructure of leakage defects was analyzed by TEM. A transversal cross-section of the region containing leakage sites was picked up by FIB milling and fixed to a

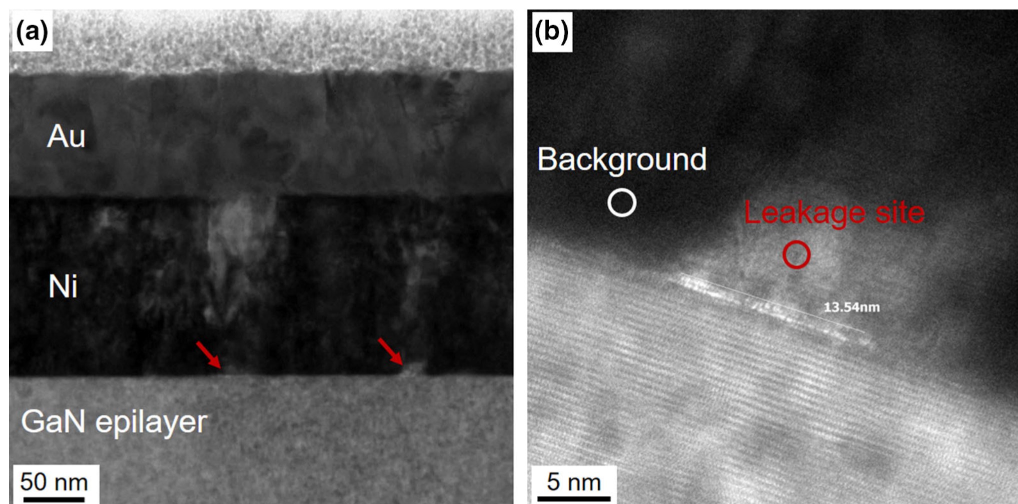

Fig. 9. Cross-sectional TEM micrographs of leakage site: (a) overall view of cross-section of Ni/GaN Schottky contact, (b) high-resolution image of leakage site at interface between Ni and GaN epilayer.

Table I. EDS elemental analysis of Ni and Ga concentration at leakage site

Element	Background (at.%)	Leakage Site (at.%)
Ni	98.02	93.52
Ga	1.98	6.48

TEM grid. Figure 9a shows a bright-field TEM micrograph of the cross-section of the Schottky contact. The Ni/GaN interface is smooth, except for a few hillocks indicated by arrows. No dislocations exist in this region. A high-resolution image of the hillock is shown in Fig. 9b. Two positions denoted in Fig. 9b were chosen for EDS elemental analysis; the results are presented in Table I, revealing that the leakage site associated with the hillock contains more Ga atoms than the background region.

DISCUSSION

First, the electrical properties of threading dislocations in GaN epilayers will be discussed. EBIC revealed that a single threading dislocation only possesses weak recombination activity, while a dislocation cluster tends to be a strong recombination center. The room-temperature EBIC contrast was weak and did not vary greatly from edge to mixed type, suggesting that dislocations are intrinsically associated with shallow levels in the bandgap. The edge or screw component had no significant effect on the intrinsic recombination activity. On the other hand, dislocation clusters with strong EBIC contrast at room temperature indicate the presence of deep levels. The origin of deep levels may be extrinsic, such as impurities. In this sense, the EBIC behavior of dislocations in GaN is analogous to that of dislocations in silicon. Intrinsically, dislocations are electrically inactive or show weak activity; when extrinsically decorated with impurities, they become active. Compared with a single dislocation, dislocation clusters tend to have a stronger capability to getter impurities. As shown herein, the formation of dislocation clusters in the epilayer is strongly affected by defects in the substrate, thus a careful choice of substrate will help to avoid the formation of dislocation clusters in the epilayer.

Second, we discuss the origin of leakage sites and their correlation with dislocations. When comparing SBDs with and without dislocation clusters, it was found that SBDs with dislocation clusters sometimes shows a relatively stronger leakage current than the latter. However, the tendency was not very clear due to the presence of other leakage sources from the electrode edge or Schottky interface. It is reported that screw-type dislocations turn out to be breakdown sites in GaN *p*–*n* junctions when biased at higher voltages such as -550 V.[12] In this study, we could not identify leakage sites at dislocations. There are two explanations for this: One is due to the limited bias range of EBIC observations. For biased EBIC observation, the bias range is limited to -50 V, beyond which the background current saturates. From another viewpoint, this provides a hint that dislocations do not act as initial leakage sites at small reverse biases. The second consideration is the different leakage mechanism of the Schottky contact versus a *p*–*n* junction. For a Schottky diode, initial leakage could easily occur due to defects at the metal/semiconductor interface. The hillocks at the Ni/GaN interface act as strong leakage sites and result in initial leakage even at small reverse bias voltages. It is considered that the Ga-rich hillocks are probably Ga-rich droplets that remained on the surface of the epilayer during its growth. Future research also suggests that, by

using a proper surface cleaning process before Ni deposition, such leakage sites could be avoided.

CONCLUSIONS

The electrical and structural properties of dislocations in vertical GaN Schottky barrier diodes are studied based on EBIC, etch pit, and TEM techniques. The dislocation type, density, and distribution are affected by defects in the substrate. A single dislocation of either edge or mixed type shows only weak EBIC contrast, indicating intrinsically weak recombination strength, whereas a dislocation cluster shows strong EBIC contrast and a deep-level recombination center may be introduced. The current leakage sites in Schottky diodes are investigated by bias-dependent EBIC. There is no direct correlation between dislocations and initial leakage sites. However, other leakage sources from grown-in pit defects and/or process-induced surface defects also exist. Three kinds of leakage/breakdown sites are found: (1) pit defects formed during epitaxial growth that act as detrimental breakdown sites, (2) leakage sites originating from the electrode periphery due to an improper lift-off process for electrode formation, and (3) leakage sites due to hillocks on the epilayer surface. These leakage sites could be avoided by improvement in the epilayer growth and device processes.

ACKNOWLEDGMENTS

This work was supported by the Ministry of Education, Culture, Sports, Science, and Technology (MEXT), Japan through its Program for research and development of next-generation semiconductor to realize energy-saving society.

REFERENCES

1. S. Fujita, *Jpn. J. Appl. Phys.* 54, 030101 (2015).
2. H. Amano, Y. Baines, E. Beam, M. Borga, T. Bouchet, P.R. Chalker, M. Charles, K.J. Chen, N. Chowdhury, R. Chu, C. De Santi, M. De Souza, S. Decoutere, L. Di Cioccio, B. Eckardt, T. Egawa, P. Fay, J.J. Freedsman, L. Guido, O. Häberlen, G. Haynes, T. Heckel, D. Hemakumara, P. Houston, J. Hu, M. Hua, Q. Huang, A. Huang, S. Jiang, H. Kawai, D. Kinzer, M. Kuball, A. Kumar, K.B. Lee, X. Li, D. Marcon, M. März, R. McCarthy, G. Meneghesso, M. Meneghini, E. Morvan, A. Nakajima, E.M.S. Narayanan, S. Oliver, T. Palacios, D. Piedra, M. Plissonnier, R. Reddy, M. Sun, I. Thayne, A. Torres, N. Trivellin, V. Unni, M.J. Uren, M. Van Hove, D.J. Wallis, J. Wang, J. Xie, S. Yagi, S. Yang, C. Youtsey, R. Yu, E. Zanoni, S. Zeltner, and Y. Zhang, *J. Phys. D Appl. Phys.* 51, 163001 (2018).
3. I.C. Kizilyalli, A.P. Edwards, O. Aktas, T. Prunty, and D. Bour, *IEEE Trans. Electron Devices* 62, 414 (2015).
4. H. Ohta, N. Kaneda, F. Horikiri, Y. Narita, T. Yashida, T. Mishima, and T. Nakamura, *IEEE Electron Device Lett.* 36, 1180 (2015).
5. A. Usui, H. Sunakawa, A. Sakai, and A.A. Yamaguchi, *Jpn. J. Appl. Phys.* 36, 899 (1997).
6. K. Motoki, T. Okahisa, S. Nakahata, N. Matsumoto, H. Kimura, H. Kasai, K. Takemoto, K. Uematsu, M. Ueno, Y. Kumagai, A. Koukitu, and H. Seki, *J. Cryst. Growth* 237–239, 912 (2002).
7. Y. Oshima, T. Eri, M. Shibata, H. Sunakawa, K. Kobayashi, T. Ichihashi, and A. Usui, *Jpn. J. Appl. Phys.* 42, L1 (2003).
8. K. Xu, J.F. Wang, and G.Q. Ren, *Chin. Phys. B* 24, 066105 (2015).
9. J. Liu, J. Huang, X. Gong, J. Wang, K. Xu, Y. Qiu, D. Cai, T. Zhou, G. Ren, and H. Yang, *CrystEngComm* 13, 5929 (2011).
10. E.G. Brazel, M.A. Chin, and V. Narayanamurti, *Appl. Phys. Lett.* 74, 2367 (1999).
11. B. Kim, D. Moon, K. Joo, S. Oh, Y.K. Lee, Y. Park, Y. Nanishi, and E. Yoon, *Appl. Phys. Lett.* 104, 102101 (2014).
12. S. Usami, Y. Ando, A. Tanaka, K. Nagamatsu, M. Deki, M. Kushimoto, S. Nitta, Y. Honda, H. Amano, Y. Sugawara, Y.Z. Yao, and Y. Ishikawa, *Appl. Phys. Lett.* 112, 182106 (2018).
13. J. Elsner, R. Jones, P.K. Sitch, V.D. Porezag, M. Elstner, T. Frauenheim, M.I. Heggie, S. Öberg, and P.R. Briddon, *Phys. Rev. Lett.* 79, 3672 (1997).
14. T. Hino, S. Tomiya, T. Miyajima, K. Yanashima, S. Hashimoto, and M. Ikeda, *Appl. Phys. Lett.* 76, 3421 (2000).
15. J.L. Weyher, S. Lazar, L. Macht, Z. Liliental-Weber, R.J. Molnar, S. Müller, V.G.M. Sivel, G. Nowak, and I. Grzegory, *J. Cryst. Growth* 305, 384 (2007).
16. L. Lu, Z.Y. Gao, B. Shen, F.J. Xu, S. Huang, Z.L. Miao, Y. Hao, Z.J. Yang, G.Y. Zhang, X.P. Zhang, J. Xu, and D.P. Yu, *J. Appl. Phys.* 104, 123525 (2008).
17. Y. Yao, Y. Ishikawa, Y. Sugawara, D. Yokoe, M. Sudo, N. Okada, and K. Tadatomo, *Superlattices Microstruct.* 99, 83 (2016).
18. P.B. Hirsch, A. Howie, P.B. Nicholson, D.W. Pashley, and M.J. Whelan, *Electron Microscopy of Thin Crystals*, 2nd ed. (Malabar: Krieger, 1977), pp. 247–275.
19. T. Sugahara, H. Sato, M.S. Hao, Y. Naoi, S. Kurai, S. Tottori, K. Yamashita, K. Nishino, L.T. Romano, and S. Sakai, *Jpn. J. Appl. Phys.* 37, L398 (1998).
20. M.A. Reshchikov and H. Morkoç, *J. Appl. Phys.* 97, 061301 (2005).
21. J.Y. Wang, Y. Oshima, Y.J. Cho, Y. Shi, and T. Sekiguchi, *Superlattices Microstruct.* 99, 77 (2016).
22. M. Albrecht, J.L. Weyher, B. Lucznik, I. Grzegory, and S. Porowski, *Appl. Phys. Lett.* 92, 231909 (2008).
23. J. Huang, K. Xu, Y.M. Fan, J.F. Wang, J.C. Zhang, and G.Q. Ren, *Nanoscale Res. Lett.* 9, 649 (2014).
24. J. Chen, W. Yi, T. Kimura, S. Takashima, M. Edo, and T. Sekiguchi, *Appl. Phys. Express* 12, 051010 (2019).
25. H.J. Leamy, *J. Appl. Phys.* 53, R51 (1982).
26. T. Sekiguchi and K. Sumino, *Rev. Sci. Instrum.* 66, 4277 (1995).
27. J. Chen, T. Sekiguchi, D. Yang, F. Yin, K. Kido, and S. Tsurekawa, *J. Appl. Phys.* 96, 5490 (2004).
28. J. Chen, T. Sekiguchi, J.Y. Li, S. Ito, W. Yi, and A. Ogura, *Appl. Phys. Lett.* 106, 102109 (2015).
29. J. Chen, T. Sekiguchi, N. Fukata, M. Takase, T. Chikyo, K. Yamabe, R. Hasunuma, Y. Akasaka, S. Inumiya, Y. Nara, and K. Yamada, *Appl. Phys. Lett.* 89, 22 (2006).
30. J. Chen and T. Sekiguchi, in *Compendium of Surface and Interface Analysis*, ed. By The Surface Science Society of Japan (Springer, Singapore, 2018), p. 149.
31. E.B. Yakimov, *J. Phys. Condens. Matter* 14, 13069 (2002).
32. E.B. Yakimov, A.Y. Polyakov, I.-H. Lee, and S.J. Pearton, *J. Appl. Phys.* 123, 161543 (2018).
33. W. Lee, H.J. Lee, S.H. Park, K. Watanabe, K. Kumagai, T. Yao, J.H. Chang, and T. Sekiguchi, *J. Cryst. Growth* 351, 83 (2012).
34. V. Voronenkov, N. Bochkareva, R. Gorbunove, P. Latyshev, Y. Lelikov, Y. Rebane, A. Tsyuk, A. Zubrilov, and Y. Shreter, *Jpn. J. Appl. Phys.* 52, 08JE14 (2013).
35. W. Yi, J. Chen, S. Higuchi, and T. Sekiguchi, *Appl. Phys. Express* 12, 051005 (2019).
36. L. Sang, B. Ren, M. Sumiya, M. Liao, Y. Koide, A. Tanaka, Y. Cho, Y. Harada, T. Nabatame, T. Sekiguchi, S. Usami, Y. Honda, and H. Amano, *Appl. Phys. Lett.* 111, 122107 (2017).

Publisher's Note Springer Nature remains neutral with regard to jurisdictional claims in published maps and institutional affiliations.